Astronomy & Astrophysics manuscript no. paper
April 11, 2009
© ESO 2009

arXiv:0904.1797v1 [astro-ph.HE] 11 Apr 2009

Multi-wavelength observations of afterglow of GRB 080319B and the modeling constraints. ⋆

S. B. Pandey[1], A. J. Castro-Tirado[2], M. Jelínek[2], Atish P. Kamble[3], J. Gorosabel[2], A. de Ugarte Postigo[4], S. Prins[5], R. Oreiro[5], V. Chantry[6], S. Trushkin[7], M. Bremer[8], J. M. Winters[8], A. Pozanenko[9], Yu. Krugly[14], I. Slyusarev[14], G. Kornienko[10], A. Erofeeva[10], K. Misra[11], A. N. Ramprakash[11], V. Mohan[11], D. Bhattacharya[11], A. Volnova[12], J. Plá[13], M. Ibrahimov[15], M. Im[16], A. Volvach[17], and R. A. M. J. Wijers[3]

[1] Aryabhatta Research Institute of Observational Sciences (ARIES), Manora Peak, Nainital, India, 263129.
[2] Instituto de Astrofísica de Andalucía (IAA-CSIC), Apartado de Correos, 3.004, E-18.080 Granada, Spain.
[3] Astronomical Institute "Anton Pannekoek", Kruislaan, 403, 1098SJ, Amsterdam, The Netherlands.
[4] European Southern Observatory, Casilla 19001, Santiago 19, Chile.
[5] Institute of Astronomy, Katholieke Universiteit Leuven, Celestijnenlaan 200D, 3001 Leuven, Belgium
[6] Institut dÁstrophysique et de Geophysique, Universite de Liege, Allee du 6 Aout 17, Sart Tilman (Bat. B5C), Liege 1, Belgium.
[7] Special Astrophysical Observatory of RAS, Nizhnij Arkhyz, Karachai-Cherkessia, 369167 Russia.
[8] Institute de Radioastronomie Millimétrique (IRAM), 300 rue de la Piscine, 38406 Saint Martin d´Héres, France.
[9] Space Research Institute of RAS, Profsoyuznaya, 84/32, Moscow 117997, Russia.
[10] Ussuriisk Astrophysical observatory, Far East Branch of RAS, Ussuriisk Region, Gornotaejnoe, 692533, Russia.
[11] Inter-University Center for Astronomy and Astrophysics (IUCAA), Pune, Ganeshkhind, Post-bag No. 4, India.
[12] Sternberg Astronomical Institute, Moscow State University, Universitetsky pr., 13, Moscow 119992, Russia.
[13] Instituto de Astrofísica de Canarias (IAC), Via Láctea s/n, E-38205 La Laguna (Tenerife), Spain.
[14] Astronomical Institute of Kharkov National University, 35 Sumskaya, Kharkov, 61022, Ukraine.
[15] Ulugh Beg Astronomical Institute, Tashkent 700052, Uzbekistan.
[16] Dept. of Physics & Astronomy, Seoul National University, 56-1 San, Shillim-dong, Kwanak-gu, Seoul, Korea.
[17] SRI Crimean Astrophysical Observatory, Nauchny, Crimea, 98409, Ukraine.

Preprint online version: April 11, 2009

ABSTRACT

Context. We present observations of the afterglow of GRB 080319B at optical, mm and radio frequencies from a few hours to 67 days after the burst.
Aims. To understand the nature of this brightest explosion based on the observed properties and it's comparison with the afterglow models.
Methods. Present observations along with other published multi-wavelength data have been used to study the light-curves and spectral energy distributions of the burst afterglow.
Results. Our results show that the observed features of the afterglow fits equally good with the Inter Stellar Matter and the Stellar Wind density profiles of the circum-burst medium. In case of both density profiles, location of the maximum synchrotron frequency ν_m is below optical and the value of cooling break frequency ν_c is below $X-$rays, $\sim 10^4$ s after the burst. Also, the derived value of the Lorentz factor at the time of naked eye brightness is ~ 300 with the corresponding blast wave size of $\sim 10^{18}$ cm.
Conclusions. The numerical fit to the multi-wavelength afterglow data constraints the values of physical parameters and the emission mechanism of the burst.

Key words. Gamma ray-bursts – afterglows – observations and models

1. Introduction

The very early time observations of Gamma-ray bursts (GRBs) during the prompt emission or during the early afterglow phase have been one of the major contributions during the *Swift* era (Zhang 2007). These observations play key role to uncover the physical mechanisms underlying these energetic cosmic explosions (Meśzaŕos 2006). The early time multi-wavelength observations are also very useful to constrain the afterglow models hence the nature of the possible progenitors and the ambient media surrounding the GRBs (Castro-Tirado et al. 1999; Piran 1999). Among the well-known examples of early observations in the pre-*Swift* era are GRB 990123 (Akerlof et al. 1999); GRB 041219 (Vestrand et al. 2005) whereas GRB 050820A (Vestrand et al. 2006); GRB 060111B (Klotz et al. 2006); GRB 060210 (Stanek et al. 2007), and GRB 071010B (Wang et al. 2008) are good examples in the post-*Swift* era. The statistics of such examples of long-duration GRBs with very early time afterglow observations have been improved because of the precise on-

Send offprint requests to: e-mail: shashi@aries.res.in

⋆ Based on observations obtained with the 0.22 m telescope at Russia the 0.7 m telescope at of Kharkov University, Ukraine, the 0.8 m telescope at Observatorio del Teide (IAC-80), Spain the 1.2 m Mercator telescope at La Palma, Spain, the 1.5 m telescope of Maidanak observatory Uzbekistan, the 2.0 m IGO Telescope at IUCAA Pune, India, the 2.5 m NOT, the PdB millimeter interferometric array France, the RATAN-600 Radio Telescope at Russia and the RT-22 radio telescope of CrAO, Ukraine.

board localization by *Swift* and co-ordinated observations with the ground based robotic optical telescopes (Gehrels et al. 2004, Gomboc et al. 2006). Out of these known examples the observed optical and γ-ray prompt emission is contemporaneous for GRB 041219 and GRB 050820A whereas for GRB 990123 and GRB 050401 the peak of the prompt optical observations have been recorded after the γ-ray emission phase.

According to the standard relativistic "Fireball" model (Rees & Meśzaŕos 1992; Meśzaŕos & Rees 1997; Panaitescu et al. 1998), the GRB prompt emission is due to the internal shocks (Narayan et al. 1992; Rees & Meśzaŕos 1994; Sari & Piran 1997a,b). The observed steep decay in the early afterglow emission, that lies between the prompt emission and the afterglow, are also explained in terms of "high latitude emission" (Nousek et al. 2006) in the case of *Swift* GRBs, irrespective of the type of shock and the radiative process involved. The very early time optical observations of several GRB afterglows are explained in terms of reverse shock (Kobayashi 2000) or/and forward shock (Rees & Meśzaŕos 1992; Katz 1994) origin. The overall afterglow behavior of long-duration GRBs including the above mentioned examples are explained in terms of "collapse of very massive stars" i.e. "Collapsars" as the most favored progenitor (MacFadyen & Woosley 1999). By now the majority of long-duration GRB afterglows have been explained in terms of constant ambient density i.e. Inter Stellar Medium (*ISM*, $\rho \propto r^0$) models (Sari, Piran, Narayan 1998; Wijers & Galama 1999; Panaitescu & Kumar 2002), although stellar wind medium (*WM*, $\rho \propto r^{-2}$) profile (Chevalier & Lee 2000a,b; Li & Chevalier 2001) are the natural consequences for the massive star environments (Zhang 2007), where ρ and r are the ambient density and the distance from the center of the progenitor star respectively. The value of ambient density is constrained by the parameters "number density" n and the "wind parameter" A_*, respectively for the *ISM* and *WM* models. Also, there are certain cases of long-duration GRB afterglows which have been explained in terms of both density profiles in form of the transition from *WM* density profile at early times to *ISM* density profile at later epochs of observations, e.g. GRB 050904 (Gendre et al. 2007) and GRB 050319 (Kamble et al. 2007).

GRB 080319B was triggered (trigger = 306757) by *Swift*-BAT (15-350 keV) at T_0=06:12:49 UT on March 19, 2008 (Racusin et al. 2008a) and was simultaneously detected by the Konus-Wind (20 keV-15 MeV) satellite (Golenetskii et al. 2008). The optical emission were started 2.75±5 s after the BAT trigger, captured by the wide field robotic telescope "Pi of the Sky" (Cwiok et al. 2007, 2008) and also by TORTORA (Molinari et al. 2006, Racusin 2008b), Raptor-Q (Wozniak et al. 2009) at later epochs. For a few seconds after the burst, the observed prompt optical flash of GRB 080319B was visible even for the unaided eye in dark skies (peaked at a visual magnitude of 5.3 around 18 s after the onset of the burst, as observed by TORTORA), breaking the record of a handful of known cases in which bright optical-*NIR* prompt emissions have been observed (Jelinek et al. 2007). *Swift*-UVOT slewed towards the burst 51 s after the trigger (Holland & Racusin 2008) and later many other ground and space based multi-wavelength facilities joined in, as summarized in detail by Bloom et al. (2009), Racusin et al. (2008b) and references therein.

The measured redshift value of the burst ($z = 0.937$, Vreeswijk et al. 2008) corresponds to a luminosity distance of $d_L = 6.01 \times 10^3$ Mpc (with the cosmological parameters $H_0 = 71$ km s^{-1}Mpc^{-1}, $\Omega_M = 0.27$, $\Omega_\Lambda = 0.73$) and an equivalent isotropic energy in γ-rays $E_{\gamma,iso} = 1.4 \times 10^{54}$ erg (20 keV − 7 MeV), which is among the highest ever measured for GRBs. The inferred high luminosity of the burst after correcting to the galactic and host extinction in the burst direction (Wozniak et al. 2009) implies that such an event could have been easily detected at redshift $z = 17$ with meter-class telescopes in the $K-$band (Bloom et al. 2009, Sagar 2005). Also, the observed value of the flux density of the optical flash of GRB 080319B ($\sim$ 20 Jy) is about 4 orders of magnitude higher than the peak flux density at the γ-rays ($\sim$ 14 mJy), the highest ever observed for GRBs (Yu et al. 2008). The significant excess of the prompt optical flux in comparison to the extrapolated γ-ray spectrum indicates different emission components for the two observed frequencies (Racusin et al. 2008b).

Thus, it is clear that multi-wavelength afterglow observations of GRB 080319B provide an unique opportunity to study the nature of this energetic cosmic explosion in detail. The observed spectral and temporal coverage of the afterglow make the burst as one of the best known examples to test the theoretical afterglow models (Pandey et al. 2003, Resmi et al. 2005). In this paper we summarize the radio, Millimeter wave (mm) and the optical observations of the afterglow in §2. The afterglow properties are discussed in §3. The modeling of the multi-wavelength afterglow data and the derived parameters are described in §4. In the last section we summarize our results in the context of observed and modeled parameters of the burst.

Table 1. Log of Millimeter wave and radio observations of the GRB 080319B afterglow. The first IRAM data point has already been published in Racusin et al. (2008b). The PdB millimeter interferometer array is in France, RATAN-600 Radio Telescope is situated close to Zelenchukskaya, Russia, and RT-22 is in Ukraine.

Start time (UT)	End time (UT)	Frequency (GHz)	Flux center (mJy)	Telescope
2008 Mar 20.0	Mar 20.5	97.0	+0.41±0.12	IRAM
2008 Mar 23.0	Mar 23.5	97.0	+0.35±0.19	IRAM
2008 Mar 27.0	Mar 27.5	97.0	+0.20±0.09	IRAM
2008 Mar 28.0	Mar 28.5	4.8	<4.0	RATAN
2008 Mar 30.0	Mar 30.5	4.8	<4.0	RATAN
2008 Apr 08.0	Apr 08.5	4.8	<3.0	RATAN
2008 May 25.0	May 25.5	2.0	<3.0	RT-22
2008 May 25.0	May 25.5	8.0	<3.0	RT-22

2. Observations

2.1. Millimeter wave and Radio Observations

Observations at millimeter frequencies of GRB 080319B afterglow were performed with the Plateau de Bure (PdB) Interferometer (Guilloteau et al. 1992) in a six-antenna extended configuration on the dates listed in Table 1. The afterglow was detected in the first round of observations starting 0.5 days after the burst and upper limits were established at later two epochs. Also, Radio observations were performed using RATAN-600 at 4.8 GHz starting 9 to 19 days after the burst and the afterglow was not detected. The afterglow was also monitored using the radio telescope RT-22/CrAO at 2.0 and 8.0 GHz on 25th May 2008. The upper limits (3σ) from RATAN-600 and RT-22/CrAO observations are also listed in Table 1.

2.2. Optical Observations

Our optical observations were performed using several Telescopes (0.22m SR-22; 0.7m AZT-8; 0.8m IAC; 1.2m

Mercator, 1.5m Maidanak (AZT-22), 2.0m IGO, 2.5m NOT(+ALFOSC)) in Far East of Russia, Europe, Middle Asia and India starting from 0.5 day to 19 days after the burst. IRAF and DAOPHOT softwares were used to perform data reduction using standard techniques. The B, V, R and I data has been calibrated using the nearby secondary standards as given in Henden (2008). The Gunn r data were calibrated using nearby calibrators. The log of our optical observations along with the details are given in Table 2.

3. Properties of the burst

3.1. Prompt emission phase

The prompt optical light-curve present a good correlation with the $\gamma-$ray light-curve, thanks to good time resolution (Racusin et al. 2008b). This correlation suggests that radiation at both frequencies originate from the same physical source under the assumptions of internal shock model (Meśzaŕos & Rees 1999; Kumar & Panaitescu 2008). There is no considerable evolution of the $X-$ray hardness ratio from very early to late times of the observations with an average photon index $\Gamma = -1.81 \pm 0.04$ (Bloom et al. 2009). There are no multi-band optical observations during the prompt emission phase of the burst. The observed spectral indices around 430s and 875s after the burst also show negligible evolution at optical frequencies (Bloom et al. 2009). The reverse shock or forward shock origin of the observed prompt optical emission is ruled out based on the observed values of temporal decay indices to be too steep than the expected one (Sari, Piran & Narayan 1998; Kobayashi 2000). Also, the observed constancy of the optical pulse width with time during the prompt emission phase (Ramirez-Ruiz & Fenimore 2000) does not support the reverse shock origin. The temporal coincidence between the prompt optical and $\gamma-$rays of the burst also indicate that they might have been originated from the same emitting region or two regions sharing the same dynamical behavior (Yu et al. 2008). The correlation of spectral lag evolution with the observed prompt optical emission of GRB 080319B also shows that they come from the same astrophysical origin and the respective radiation mechanisms were dynamically coupled (Stamatikos et al. 2009). Furthermore, the significant excess of the prompt optical flux in comparison to the extrapolated γ-ray spectrum to the optical frequencies possibly indicate towards two different emission components for the two observed frequencies (but see Kumar & Panaitescu 2008).

3.2. Multi-frequency evolution of the afterglow

According to the standard Fireball model, the GRB afterglow is expected to be synchrotron radiation with the observed flux $f \propto \nu^{\beta} t^{\alpha}$, for the regions without spectral breaks, where the values of power-law temporal decay index (α) and spectral index (β) are related to each other and can be used to understand the afterglow evolution (Sari, Piran, Narayan 1998; Sari, Piran, Halpern 1999). The rich multi-frequency data of the afterglow of GRB 080319B available in the literature and the data from the present work are used to measure the indices α and β of the afterglow. The values of the temporal decay indices have been derived using empirical broken power-law relations by minimization of χ^2 as described in Granot & Sari (2002) (their equations 1 and 4). The bright optical flash ($10 < t < 100$ s) rises to the peak brightness ($V \sim 5.32 \pm 0.04$) with $\alpha_{V1} = 4.64 \pm 0.67$, and after about 50 s decays with $\alpha_{V2} = -4.41 \pm 0.10$. Post ~ 100 s decay of the optical afterglow could be described as broken power law with $\alpha_{V3} = -2.33 \pm 0.23$, $\alpha_{V4} = -1.31 \pm 0.02$ and the break happening at $\sim 784.9 \pm 304.4$ s after the burst. The $X-$ray afterglow light curve is described by a triple broken power law with $\alpha_{X1} = -1.40 \pm 0.01$, $\alpha_{X2} = -1.94 \pm 0.12$, $\alpha_{X3} = -1.14 \pm 0.09$, $\alpha_{X4} = -2.67 \pm 0.74$ and the breaks happening at $t_{b,X1} = 2583.39 \pm 871$ s, $t_{b,X2} = (3.99 \pm 0.89) \times 10^4$ s and $t_{b,X3} = (1.0 \pm 0.29) \times 10^6$ s with $\chi^2/dof = 975/710 = 1.37$. The derived values of $X-$ray temporal index α_{X4} and the corresponding break time are in agreement with those derived by Tanvir et al. (2009) using late time $X-$ray and optical data which provide evidences in favor of jet-break around $\sim 10^6$ s after the burst.

4. Discussion

4.1. Surrounding medium

The closure relations between α and β can also be used to infer density profile of the circum-burst medium or to distinguish between theoretical afterglow models like *ISM* and *WM* (Price et al. 2002; Starling et al. 2008). For the radiation due to a shock wave interacting with the *ISM* circum-burst medium, the expected closure relation is $\alpha - 1.5\beta = 0.0$ in a spectral regime $\nu_m < \nu < \nu_c$, where ν_m and ν_c are the maximum synchrotron and cooling frequencies , respectively. In the case of *WM* circum-burst medium and for a spectral regime $\nu_m < \nu < \nu_c$ the closure relation is $\alpha - 1.5\beta = 0.5$. If $\nu_m < \nu_c < \nu$ then $\alpha - 1.5\beta = -0.5$ is expected irrespective of the density profile being *ISM* or *WM*. At early times ($t \leq 2000$ s), the optical afterglow is dominated by emission due to the reverse shock and at late times ($t \geq 10^5$ s) it is clearly dominated by that due to the forward shock. The values of β estimated by Bloom et al.(2009) and the values of α of optical light curves at ($t > 10^5$ s) are consistent with the closure relations for both the density profiles, *ISM* and *WM* with the spectral regime being $\nu_m < \nu_{optical} < \nu_c$.

Also, It is clear that the temporal decay index of the optical afterglow between 100 s and 1000 s ($\alpha \sim -2.3$) is faster than what would be expected due to a forward shock scenario ($\alpha \sim -0.8$) interacting with the circum-burst medium (Sari, Prian & Narayan 1998). However, such a steep decay would be expected due a reverse shock interacting with the ejected shell. In that case, the radiation due to interaction of the forward shock with circum-burst medium would dominate the afterglow after the radiation from reverse shock has died-down considerably which in this case could be happening after 10^5 s. Thus, this optical afterglow could be explained using the reverse shock and the forward shock interactions with the circum-burst medium.

4.2. Numerical model fits to the data

We have fitted the afterglow using a reverse shock (RS) model, a forward shock (FS) model and the radiation mechanism assumed is synchrotron following the standard Fireball scenario (Rees & Meśzaŕos 1992; Meśzaŕos & Rees 1994; Kobayashi 2000). As shown in Figure (1), the multi-band optical afterglow is very well reproduced by this model whereas $X-$ray observations can not be reproduced by the model. Our best fit model is consistent with no jet break in the optical afterglow and introducing a jet break at $t \sim 10^6$ s to coincide with the break in the $X-$ray afterglow does not change the fits significantly.

The complicated behavior of the $X-$ray afterglow has been explained by Racusin et al. (2008b) using a two-component jet model - a central narrow jet surrounded by a co-axial wider jet. In this model, the $X-$ray afterglow from the central narrow jet dominates at early times, until about 2×10^4 s, when

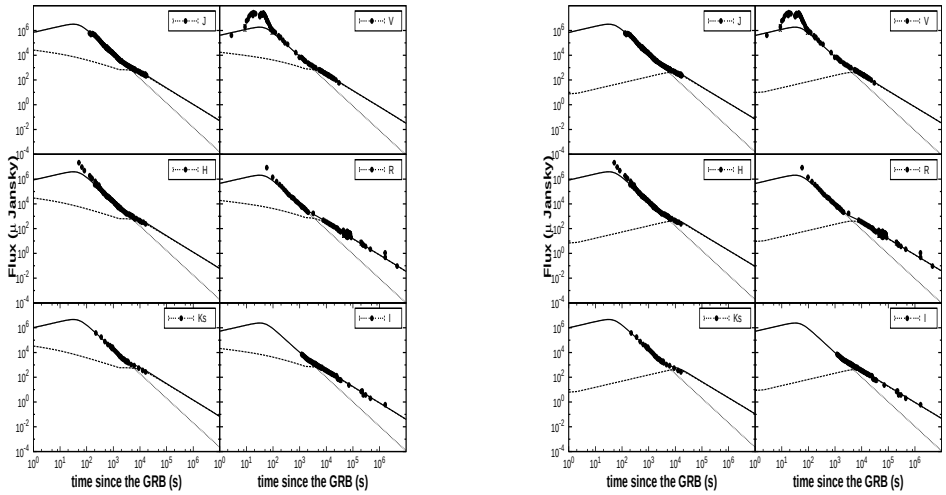

Fig. 3. The contributions due to the RS and FS to the afterglow of GRB 080319B at optical-*NIR* bands are represented by using the dashed and dotted lines respectively. The addition of the two components is shown using the solid line. The left and right panels are *WM* and *ISM* models, respectively.

it fades below the brightness of the surrounding wide jet. In this model, the breaks in the $X-$ray afterglow light-curves at times $t_{b,X1} \sim 2\times10^3$ *s* and $t_{b,X3} \sim 10^6$ *s* correspond to the jet breaks due to the lateral spreading of narrow and wide jets, respectively. We have tried to fit the whole data set using this two-component-jet model also, but we found that in this model the optical radiation from the narrow jet would be brighter than the observed optical afterglow (See Figure 2). There is no possible way to suppress this optical radiation from the narrow jet. The dominance of RS over FS contribution at early times of the light-curves are also shown for optical-*NIR* frequencies in Figure 3 for both the models.

Alternatively, it is possible that the $X-$ray and optical afterglows of GRB 080319B are not related to each other and may have independent origins. Also, the X-ray afterglow predicted by the RS-FS model is fainter than that is observed and requires an additional component.

Assuming that the shock-wave is expanding into the circum-burst medium which has a *WM* density profile, our best fit spectral parameters at epoch $t = 10^4$ *s* imply that the peak of the synchrotron spectrum is below the optical bands ($\nu_m < 1.3\times10^{14}$ Hz) with corresponding normalization flux ($F_{\nu_m} < 607\ \mu$Jy) and the self-absorption frequency, $\nu_a > 10^8$ Hz. The index of electron energy distribution $p \sim 2.07$ is lower than the canonical value $p \sim 2.3$ which has normally been observed (Panaitescu & Kumar 2001, 2002; Starling et al. 2008). The location of the cooling break frequency can be constrained to be below the $X-$ray band $\nu_c \leq 10^{18}$ Hz which would be consistent with the observed $X-$ray afterglow at late times ($t > 10^5$ *s*). However, if origin of the $X-$ray afterglow is independent of the optical afterglow then $\nu_c \ll 10^{18}$ Hz.

The estimated isotropic equivalent afterglow kinetic energy (E_K^{iso}) released in this explosion turns out to be $< 5.5\times10^{53}$ erg. For the assumed *WM* circum-burst medium we find the value of the parameter $A_* > 0.01$. The fraction of the total energy given for accelerating electrons (ϵ_e) and into the magnetic fields (ϵ_B) turn out to be about > 0.41 and $< 3\times10^{-3}$, respectively. The absence of any jet break until about 10^6 *s* imply a jet opening angle > 1.4 degrees and hence the true amount of released energy must be $> 8\times10^{49}$ erg. The radius of the Fireball at 10^4 *s* turns out to be $< 5\times10^{18}$ cm which we extrapolated back in time to estimate the physical size of the emitting region during the optical flash ($t \sim 50$ *s*) and it turns out to be $< 3.6\times10^{17}$ cm. Similarly, the Lorentz factor of the blast-wave turns out to be < 64 at 10^4 *s* after the burst which corresponds to the Lorentz factor of about < 240 at the time of the optical flash. These findings, which are based only on the evolution of the afterglow, are comparable with those of Racusin et al. (2008b) and Kumar & Panaitescu (2008) who have used arguments based on the prompt emission to reach these conclusions. It is reassuring that the different approaches have resulted in similar Fireball sizes and the blast wave Lorentz factors.

The afterglow can also be explained by assuming *ISM* density profile of the circum-burst medium. The best fit spectral parameters in this case, at epoch $t = 10^4$ *s* turn out to be $\nu_m < 2.1\times10^{14}$ Hz with corresponding flux $F_{\nu_m} < 566\ \mu$Jy, and the self-absorption frequency, $\nu_a > 10^8$ Hz. To explain relatively steep decay of the afterglow the required value of $p = 2.71$ turn out to be on a higher side and $\nu_c \leq 10^{18}$ Hz, similar as in the case of *WM* density profile.

The physical parameters estimated using these best fit spectral parameters are $E_K^{iso} < 2.4\times10^{52}$ erg, $\epsilon_e > 0.14$, $\epsilon_B < 0.02$ and $n > 7.5\times10^{-4}$ atoms/cc. The absence of any jet break until about 10^6 *s* means that the jet opening angle $\theta_j > 4.6$ degrees and hence the beaming corrected afterglow kinetic energy $E_K^{corr} > 3.8\times10^{49}$ erg. The radius of the Fireball at 10^4 *s* turns out to be about $< 2.1\times10^{18}$ cm and at the time of the optical flash $t \sim 50$ *s* about $< 5.5\times10^{17}$ cm. The corresponding Lorentz factors being < 52.4 and < 382, at 10^4 *s* and at 50 *s* after the burst receptively. As before, these values are also comparable to those of Racusin et al. (2008) and Kumar & Panaitescu (2008).

5. Conclusions

Observations of the afterglow of GRB 080319B at radio, mm and optical frequencies are presented. The simultaneous multi-band afterglow modeling is useful to constrain the nature of the burst emission mechanism and the ambient medium. We find that the afterglow of GRB 080319B is consistent with the fireball expanding either into the *ISM* or into the *WM* circum-burst

medium. We also rule out the double-jet model as a correct explanation for the observed multi-band behavior of the afterglow. While under the assumptions of our model we are able to explain the multi-band optical and radio afterglow reasonably well, we find that the X-ray afterglow is difficult to explain. Alternatively, it is possible that the optical and $X-$ray afterglows might have different origins. The Lorentz factor of the shock wave is estimated entirely from the afterglow evolution. The Lorentz factor at the time of naked eye brightness, extrapolated from the late estimation, turns out to be ~ 300. The corresponding radius of the shock front is about 10^{17} cm. We also showed that the early peak brightness of the afterglow could not be due to the reverse shock. An additional emission mechanism, such as internal shocks, is required. The results also indicate that existing blast-wave afterglow models are required to be modified in the light of complicated behavior of observed afterglows. In future, observations of prompt optical spectra will be very useful to understand the very early part of the afterglows of GRBs.

Acknowledgements. This research has made use of data obtained through the High Energy Astrophysics Science Archive Research Center On Line Service, provided by the NASA/Goddard Space Flight Center. Partly supported by the Spanish Ministry program AYA 2007-63677. SBP acknowledge the Indo-Russian (DST-RFBR) project No. RUSP-836 (RFBR-08-02:91314) for this research work and Prof. V. V. Sokolov for the useful discussions. The co-author VC, a Research Fellow, acknowledges the Belgian National Fund for Scientific Research (FNRS) for the financial support. Observation in Ussuriisk Astrophysical Observatory was made with RS-22 telescope provided by ISON.

References

Akerlof C., Balsano R., Barthelmy S. et al. 1999, Nature, 398, 400
Band D., Matteson, J., Ford, L. et al., 1993, ApJ, 413, 281
Bloom J., Perley, D. A., Li, W. et al., 2009, ApJ, 691, 723
Castro-Tirado A. J. et al., 1999, Science, 283, 2069
Chevalier R. A. & Li Z., 2000a, ApJ, 520, L29
Chevalier R. A. & Li Z., 2000b, ApJ, 536, 195
Cwiok M., Dominik W., MaÅek K. et al., 2007, Ap&SS, 309, 531
Cwiok M., Dominik W., Kasprowicz G. et al., 2008, GCNC 7439
Gehrels N., Chincarini G., Giommi P., 2004, ApJ, 611, L1005
Gendre B., Galli A., Corsi A. et al., 2007, A&A, 462, 565
Golenetskii S., Aptekar R, Mazets E. et al., 2008, GCNC 7482
Gomboc A., Guidorzi, C., Mundell, C. G, 2006, NCimB, 121, 1303
Granot J. & Sari R., 2002, ApJ, 568, 820
Guilloteau S., Delannoy J., Downes, D. et al., 1992, A&A, 262, 624
Henden A., 2008, GCNC 7528
Holland S. T. & Racusin J. L., 2008, GCNC 7496
Jelinek M., Prouza M., Kubanek P. et al., 2006, A&A, 454, L119
Kamble A. P., Resmi L. & Misra P., 2007, ApJ, 664, L5
Katz J. I., 1994, ApJ, 422, 248
Klotz A., Gendre B., Stratta G. et al. 2006, A&A, 451, L39
Kobayashi S., 2000, ApJ, 545, 507
Kumar P. & Panaitescu A., 2008, MNRAS, 391, L19
Li Z. & Chevalier R. A., 2001, ApJ, 551, 940
MacFadyan A. I. & Woosley S. E., 1999, ApJ, 524, 262
Meśzaŕos P., 2006, Rep. Prog. Phys. 69:2259-2321
Meśzaŕos P. & Rees M. J., 1994, MNRAS, 269, L41
Meśzaŕos P. & Rees M. J., 1997, ApJ, 476, 232
Meśzaŕos P. & Rees M. J., 1999, MNRAS, 306, L39
Molinari E., Bondar S., Karpov S. et al., 2006, Nuovo Cimento, 121, 1525
Nousek J., Kouveliotou C., Grupe D. et al., 2006, ApJ, 642, 389
Panaitescu A., Meśzaŕos P. & Rees M. J., 1998, ApJ, 503, 314
Panaitescu A. & Kumar P., 2001, ApJ, 560, L49
Panaitescu A.,& Kumar P., 2002, ApJ, 571, 779
Pandey S. B., Sahu D. K., Resmi L et al., 2003, BASI, 31, 19
Price P. A., Berger E., Reichart D. E. et al. 2002, ApJ, 572, L51
Piran T. 1999, Physics Reports, 314, 575
Racusin J. L., Gehrels N., Holland S. T., et al., 2008a, GCNC 7427
Racusin J. L., Karpov S. V., Sokolowski M. et al., 2008b, Nature, 455, 183
Ramirez-Ruiz E. & Fenimore E. E., 2000, ApJ, 539, 712
Rees M. J. & Meśzaŕos P., 1992, MNRAS, 258, L41
Resmi L., Ishwara C. H., Castro-Tirado A. J. et al., 2005, A&A, 440, 477
Sagar R, 2005, BASI, 33, 352
Sari R. & Piran T., 1997a, ApJ, 485, 270
Sari R. & Piran T., 1997b, MNRAS, 287, 110
Sari R., Piran T. & Narayan R., 1998, ApJ, 497, L17
Sari R., Piran T. & Halpern J. P., 1999, ApJ, 519 L17
Stamatikos M., Ukwatta T. N., Sakamoto T. et al., 2009, astro-ph/08092132v1
Stanek K. J., Dai X., Prieto J. L., et al. 2007, ApJ, L21
Starling R. L. C., Van Der Horst A. J., Rol E. et al. 2008, ApJ, 672, 433
Tanvir N. R., Evert R., Andrew L. et al., 2009, Submitted to ApJ, astro-ph/08121217
Vestrand W. T., Wozniak, P. R., Wren, J. A. et al., 2005, Nature, 435, 178
Vestrand W. T., Wren, J. A., Wozniak, P. R. et al., 2006, Nature, 442, 172
Vreeswijk P. M., Smette A., Malesani D. et al., 2008, GCNC 7451
Wang J. H., Schwamb M. E., Huang K. Y. et al., 2008, ApJ, 679, L5
Wijers R. A. M. J & Galama T. J., 1999, ApJ, 523, 177
Wozniak P. R., Vestrand W. T., Panaitescu A. et al, 2009, ApJ, 691, 495
Yu Y. W., Wang X. Y., Dai Z G.. 2008, astro-ph/08062010
Zhang, B, 2007, Chinese Journal of Astronomy and Astrophysics, 7, 1

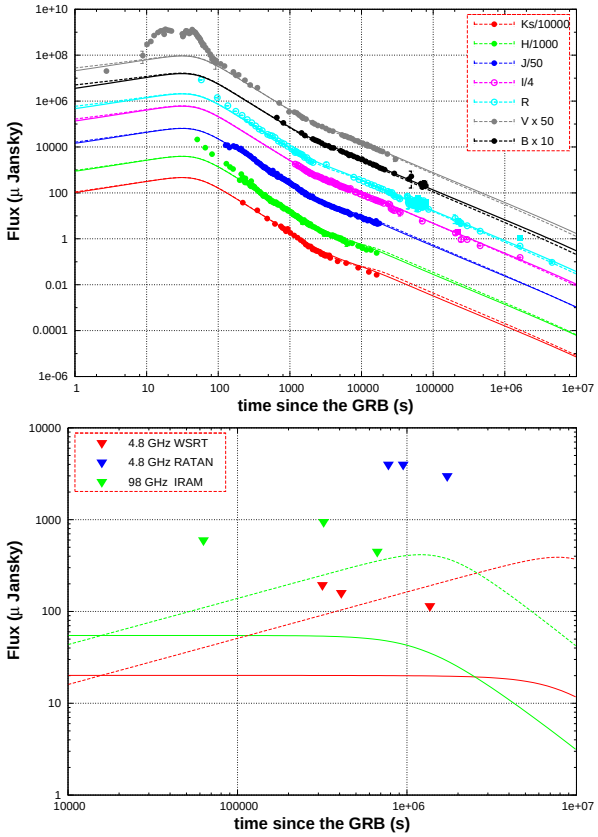

Fig. 1. Light curves of the afterglow of GRB 080319B : The optical-*NIR* and $X-$ray afterglow is shown in the top panel and the radio data in the bottom panel. The present optical observations are plotted along with other published optical and $X-$ray data, taken from the literature (Bloom et al. 2009, Racusin et al. 2008b). The FS-RS model is used to fit the afterglow light curves. The solid lines in the plots represent the resultant best fit *WM* model whereas dotted line show the best fit *ISM* model. The radiation due to the RS peaks around $\sim$ 50 *s* and dominates the afterglow up to a few thousand seconds. We have considered the case of 'Thick Shell' as discussed in Kobayashi et al.(2000) to calculate the RS afterglow. The optical band is assumed to be between the ν_m^{RS} and ν_c^{RS} i.e. the values of ν_m and ν_c during the reverse shock phase respectively and the value of electron energy distribution index to be $p = 2.32$. It can be clearly seen from the plots that the optical flash corresponding to the 'naked eye' brightness of the afterglow can not be explained as being due the RS. The decline of the *R* and *H* bands brightness before a few hundred seconds is faster than that predicted by the RS-FS model used here. This could be the high-latitude emission from the optical flash. The FS radiation starts dominating the optical light curves after about a few thousand seconds. There is no sign of any jet break at least until about 10^6 *s*. The predicted model results at $X-$ray frequencies are also plotted along with the observed $X-$ray light-curve (solid squares), showing clear deviations. The bottom panel shows the radio-mm observations of the afterglow. The inverted triangles represent the 5σ upper limits on the afterglow flux and the solid lines are the best fit estimates of the afterglow flux due to the FS. The radio afterglow due to the RS is expected to have died down significantly by the time the radio observations were conducted.

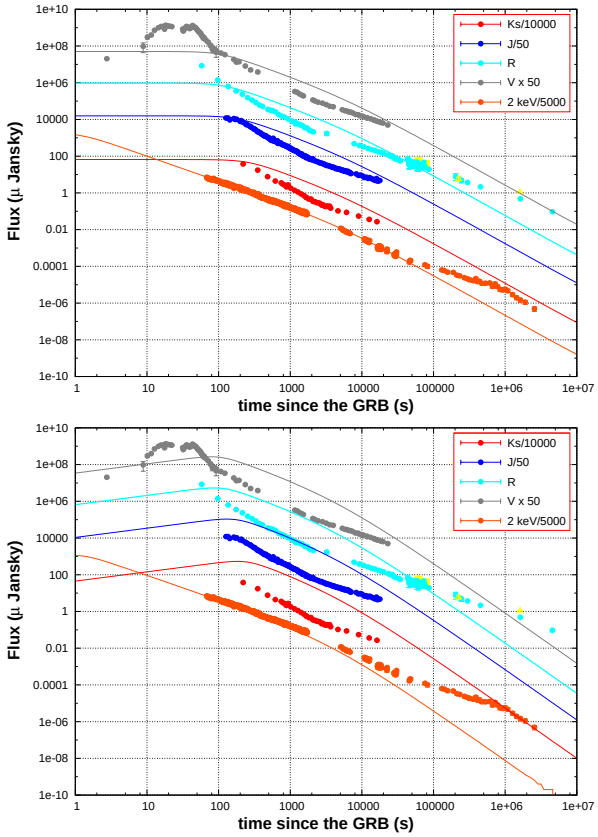

Fig. 2. The afterglow of GRB 080319B - a comparison with the double jet model: The model light-curves shown in top and bottom panels are plotted for the *WM* and *ISM* cases, respectively. The model here assumes the double jet scenario. The contribution to the afterglow only due to the narrow jet is shown in the figure. The narrow jet is assumed to be responsible for the the early $X-$ray afterglow. The estimated optical radiation due to the narrow jet is much brighter than the observed optical afterglow, which invalidates the double jet model (Racusin et al. 2008b) for GRB 080319B.

Table 2. Log of optical-*NIR* observations of the afterglow of GRB 080319B.

$UT\,start[d]$	$T-T_0[d]$	T_{exp}	$Filter$	mag	err_{mag}	$Telescope$
2008 Mar. 19.4616	0.2027	1200 s	none	>15.5		0.22 m SR-22
2008 Mar. 19.7642	0.5052	600 s	R	19.07	0.19	0.7 m AZT-8
2008 Mar. 19.7721	0.5132	600 s	R	19.26	0.27	0.7 m AZT-8
2008 Mar. 19.7800	0.5211	600 s	R	19.74	0.50	0.7 m AZT-8
2008 Mar. 19.7911	0.5322	600 s	R	19.96	0.39	0.7 m AZT-8
2008 Mar. 19.7974	0.5385	600 s	R	19.60	0.34	0.7 m AZT-8
2008 Mar. 19.8055	0.5466	900 s	R	19.60	0.20	0.7 m AZT-8
2008 Mar. 19.8174	0.5585	900 s	R	19.40	0.15	0.7 m AZT-8
2008 Mar. 19.8285	0.5696	900 s	R	19.89	0.28	0.7 m AZT-8
2008 Mar. 19.8470	0.5881	900 s	R	19.82	0.23	0.7 m AZT-8
2008 Mar. 19.8557	0.5968	900 s	R	20.06	0.19	0.7 m AZT-8
2008 Mar. 19.8630	0.6041	900 s	R	19.88	0.23	0.7 m AZT-8
2008 Mar. 19.8888	0.6299	720 s	R	20.00	0.27	0.7 m AZT-8
2008 Mar. 19.8980	0.6391	720 s	R	19.52	0.16	0.7 m AZT-8
2008 Mar. 19.9071	0.6482	720 s	R	20.09	0.28	0.7 m AZT-8
2008 Mar. 19.9139	0.6550	720 s	R	19.80	0.24	0.7 m AZT-8
2008 Mar. 19.9234	0.6645	900 s	R	19.88	0.27	0.7 m AZT-8
2008 Mar. 19.9354	0.6765	900 s	R	20.19	0.40	0.7 m AZT-8
2008 Mar. 19.9497	0.6908	900 s	R	19.54	0.15	0.7 m AZT-8
2008 Mar. 19.9625	0.7036	900 s	R	20.16	0.44	0.7 m AZT-8
2008 Mar. 19.9752	0.7163	720 s	R	20.47	0.25	0.7 m AZT-8
2008 Mar. 19.9843	0.7254	960 s	R	20.00	0.37	0.7 m AZT-8
2008 Mar. 19.9959	0.7370	900 s	R	20.03	0.37	0.7 m AZT-8
2008 Mar. 20.0127	0.7538	720 s	R	20.01	0.22	0.7 m AZT-8
2008 Mar. 20.0196	0.7607	720 s	R	19.83	0.21	0.7 m AZT-8
2008 Mar. 20.0664	0.8075	720 s	R	19.94	0.23	0.7 m AZT-8
2008 Mar. 20.0755	0.8166	720 s	R	20.22	0.26	0.7 m AZT-8
2008 Mar. 20.0848	0.8259	900 s	R	20.28	0.24	0.7 m AZT-8
2008 Mar. 20.0959	0.8370	900 s	R	19.74	0.16	0.7 m AZT-8
2008 Mar. 20.1069	0.8480	600 s	R	19.56	0.20	0.7 m AZT-8
2008 Mar. 19.8319	0.5730	600 s	V	19.60	0.70	0.7 m AZT-8
2008 Mar. 20.0870	0.8351	1200 s	I	19.57	0.08	0.8 m IAC 80
2008 Mar. 19.9924	0.7457	4×300 s	R	19.82	0.07	0.8 m IAC 80
2008 Mar. 20.0557	0.8003	600 s	R	19.94	0.11	0.8 m IAC 80
2008 Mar. 20.1067	0.8548	2×600 s	R	20.15	0.08	0.8 m IAC 80
2008 Mar. 20.1294	0.8778	2×600 s	R	20.14	0.09	0.8 m IAC 80
2008 Mar. 20.2454	0.9972	3×600 s	R	20.50	0.08	0.8 m IAC 80
2008 Mar. 22.0730	2.8355	6×600 s	R	22.03	0.27	0.8 m IAC 80
2008 Mar. 20.0252	0.7814	(1200+600) s	V	20.39	0.10	0.8 m IAC 80
2008 Mar. 20.0648	0.8165	3×600 s	B	20.89	0.12	0.8 m IAC 80
2008 Mar. 20.1703	0.9149	600 s	B	20.75	0.20	0.8 m IAC 80
2008 Mar. 19.9361	0.6985	120 s	r	19.56	0.17	1.2 m Mercator
2008 Mar. 19.9613	0.7031	120 s	r	19.28	0.19	1.2 m Mercator
2008 Mar. 19.9631	0.7049	120 s	r	19.74	0.15	1.2 m Mercator
2008 Mar. 19.9649	0.7067	120 s	r	19.37	0.11	1.2 m Mercator
2008 Mar. 19.9667	0.7085	120 s	r	19.93	0.15	1.2 m Mercator
2008 Mar. 19.9681	0.7095	60 s	r	19.53	0.11	1.2 m Mercator
2008 Mar. 19.9691	0.7106	60 s	r	20.07	0.21	1.2 m Mercator
2008 Mar. 19.9702	0.7117	60 s	r	19.41	0.10	1.2 m Mercator
2008 Mar. 19.9713	0.7127	60 s	r	19.66	0.20	1.2 m Mercator
2008 Mar. 19.9723	0.7138	60 s	r	19.82	0.15	1.2 m Mercator
2008 Mar. 19.9734	0.7148	60 s	r	19.68	0.09	1.2 m Mercator

$UT\,start[d]$	$T-T_0[d]$	$T_{\rm exp}$	$Filter$	mag	err_{mag}	$Telescope$
2008 Mar. 19.9745	0.7159	60 s	r	19.61	0.09	1.2 m Mercator
2008 Mar. 19.9759	0.7177	120 s	r	19.57	0.12	1.2 m Mercator
2008 Mar. 19.9777	0.7195	120 s	r	19.54	0.09	1.2 m Mercator
2008 Mar. 19.9794	0.7212	120 s	r	19.62	0.07	1.2 m Mercator
2008 Mar. 19.9812	0.7230	120 s	r	19.83	0.09	1.2 m Mercator
2008 Mar. 19.9830	0.7248	120 s	r	19.58	0.06	1.2 m Mercator
2008 Mar. 19.9848	0.7266	120 s	r	19.65	0.07	1.2 m Mercator
2008 Mar. 19.9865	0.7283	120 s	r	19.67	0.07	1.2 m Mercator
2008 Mar. 19.9883	0.7301	120 s	r	19.78	0.08	1.2 m Mercator
2008 Mar. 19.9900	0.7318	120 s	r	19.51	0.07	1.2 m Mercator
2008 Mar. 19.9918	0.7336	120 s	r	19.66	0.08	1.2 m Mercator
2008 Mar. 19.9936	0.7354	120 s	r	19.47	0.05	1.2 m Mercator
2008 Mar. 19.9953	0.7371	120 s	r	19.62	0.06	1.2 m Mercator
2008 Mar. 19.9971	0.7389	120 s	r	19.46	0.05	1.2 m Mercator
2008 Mar. 19.9989	0.7407	120 s	r	19.62	0.06	1.2 m Mercator
2008 Mar. 20.1446	0.8871	120 s	r	19.76	0.07	1.2 m Mercator
2008 Mar. 20.1464	0.8888	120 s	r	19.95	0.08	1.2 m Mercator
2008 Mar. 20.1481	0.8906	120 s	r	20.14	0.10	1.2 m Mercator
2008 Mar. 20.1500	0.8925	120 s	r	19.78	0.07	1.2 m Mercator
2008 Mar. 20.1517	0.8942	120 s	r	20.04	0.11	1.2 m Mercator
2008 Mar. 20.1535	0.8960	120 s	r	19.98	0.10	1.2 m Mercator
2008 Mar. 20.1554	0.8979	120 s	r	19.85	0.08	1.2 m Mercator
2008 Mar. 20.1572	0.8997	120 s	r	19.85	0.12	1.2 m Mercator
2008 Mar. 20.1589	0.9014	120 s	r	19.87	0.13	1.2 m Mercator
2008 Mar. 20.1607	0.9032	120 s	r	19.87	0.11	1.2 m Mercator
2008 Mar. 20.1625	0.9049	120 s	r	19.92	0.09	1.2 m Mercator
2008 Mar. 20.1642	0.9067	120 s	r	19.96	0.11	1.2 m Mercator
2008 Mar. 20.1660	0.9085	120 s	r	20.04	0.10	1.2 m Mercator
2008 Mar. 20.1678	0.9103	120 s	r	19.84	0.08	1.2 m Mercator
2008 Mar. 20.1695	0.9120	120 s	r	19.73	0.09	1.2 m Mercator
2008 Mar. 20.1713	0.9138	120 s	r	19.84	0.11	1.2 m Mercator
2008 Mar. 20.1731	0.9156	120 s	r	19.92	0.10	1.2 m Mercator
2008 Mar. 20.1748	0.9173	120 s	r	20.01	0.12	1.2 m Mercator
2008 Mar. 20.1766	0.9191	120 s	r	19.91	0.10	1.2 m Mercator
2008 Mar. 20.1784	0.9208	120 s	r	20.08	0.09	1.2 m Mercator
2008 Mar. 20.1801	0.9226	120 s	r	19.71	0.07	1.2 m Mercator
2008 Mar. 20.1819	0.9244	120 s	r	19.87	0.09	1.2 m Mercator
2008 Mar. 20.1837	0.9261	120 s	r	19.83	0.07	1.2 m Mercator
2008 Mar. 20.1854	0.9279	120 s	r	19.84	0.09	1.2 m Mercator
2008 Mar. 21.8618	2.6029	5760 s	I	21.22	0.15	1.5 m AZT-22
2008 Mar. 21.8781	2.6192	5610 s	R	21.81	0.26	1.5 m AZT-22
2008 Apr. 07.0086	18.7479	7200 s	R	>23.6		1.5 m AZT-22
2008 Mar. 19.9179	0.6590	3×600 s	R	19.66	0.09	2.0 m IGO
2008 Mar. 27.9511	8.6524	28×120,s	R	>23.0		2.5 m NOT

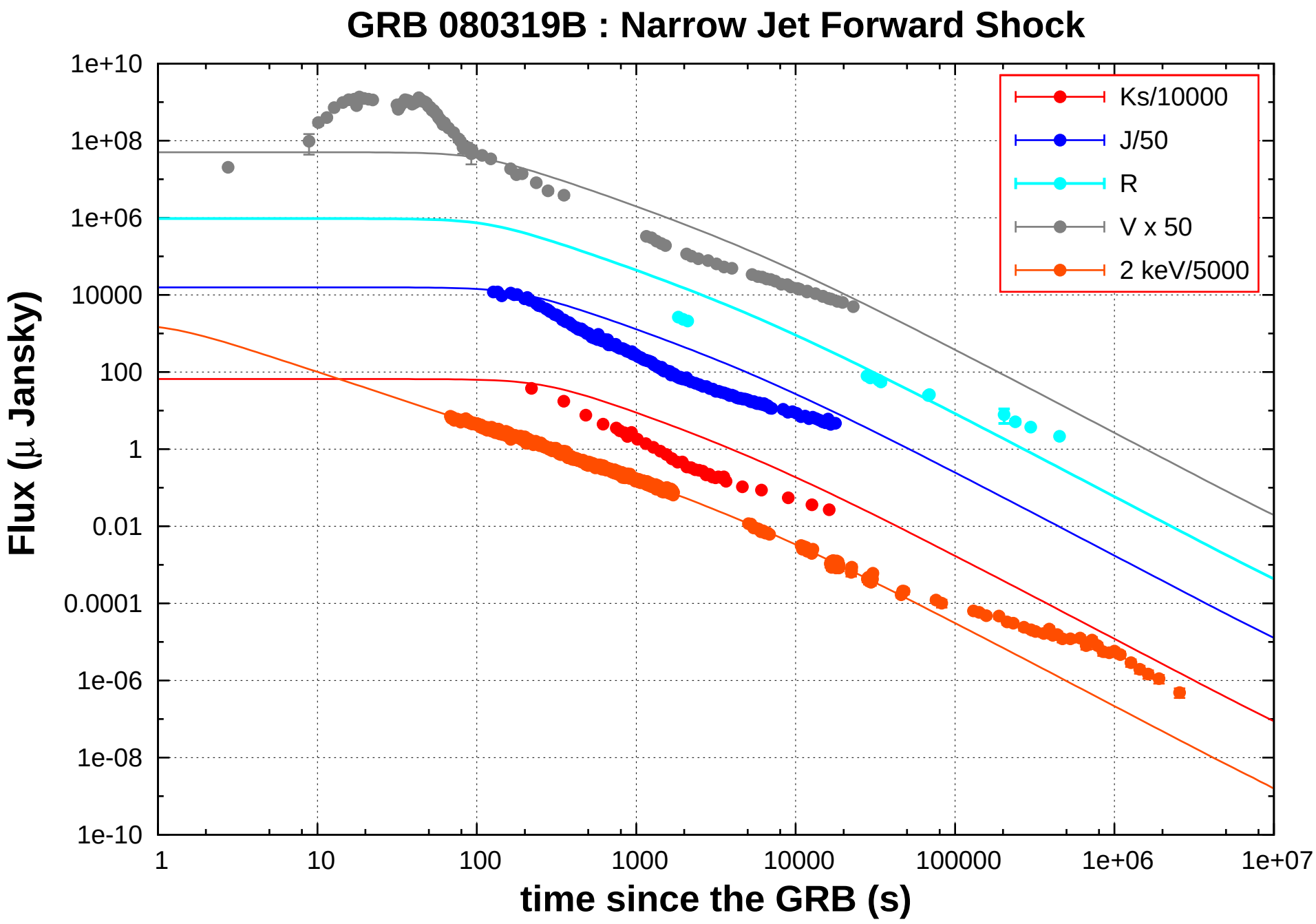
GRB 080319B : Narrow Jet Forward Shock
Flux (μ Jansky)
time since the GRB (s)
1e+10
1e+08
1e+06
10000
100
1
0.01
0.0001
1e-06
1e-08
1e-10
1
10
100
1000
10000
100000
1e+06
1e+07
Ks/10000
J/50
R
V x 50
2 keV/5000

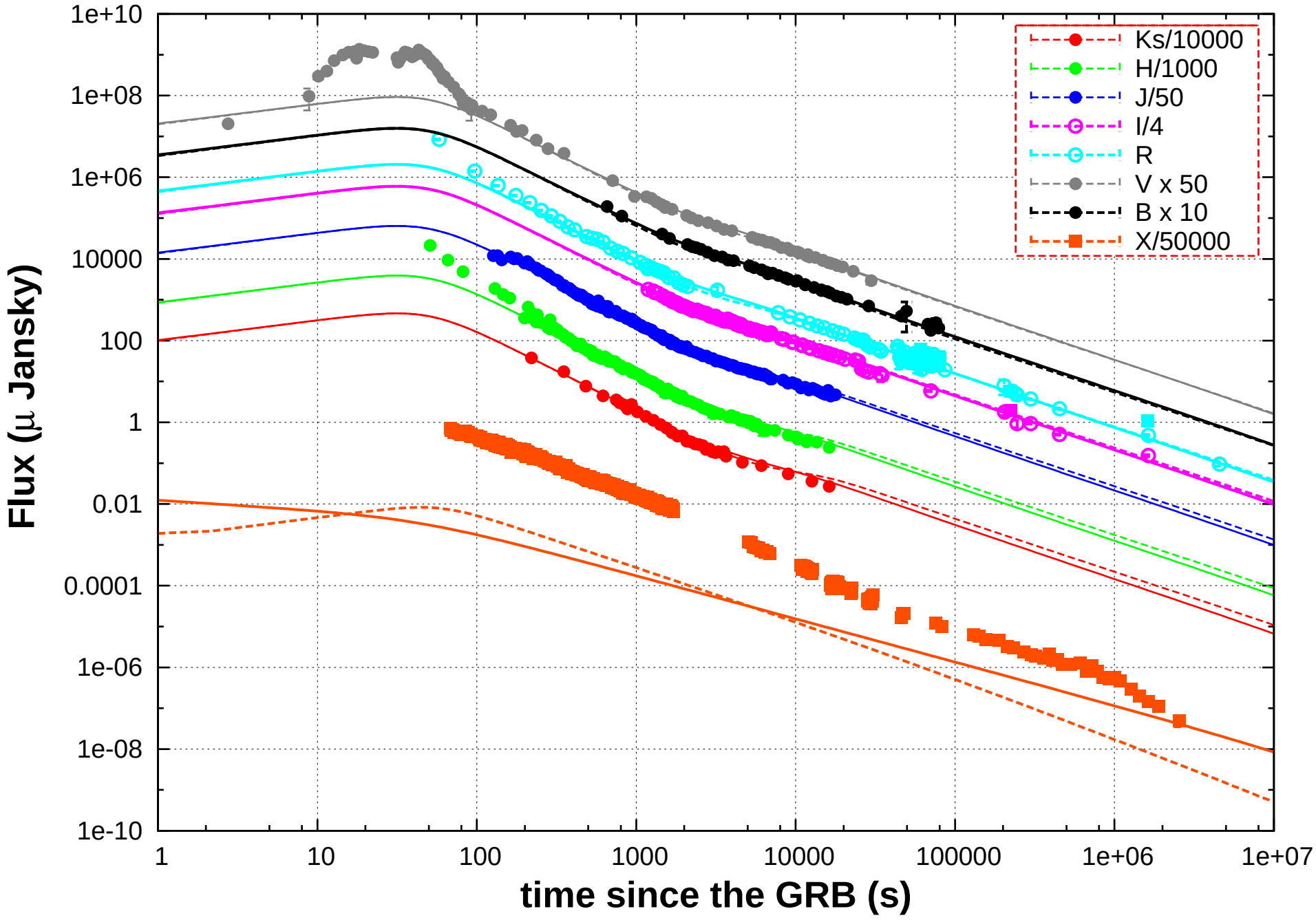
Ks/10000
H/1000
J/50
I/4
R
V x 50
B x 10
X/50000
Flux (μ Jansky)
time since the GRB (s)
1e+10
1e+08
1e+06
10000
100
1
0.01
0.0001
1e-06
1e-08
1e-10
1
10
100
1000
10000
100000
1e+06
1e+07